Smart Structures and Systems, *Vol. 27, No. 2 (2021) 365-378*
DOI: https://doi.org/10.12989/sss.2021.27.2.365

Experimental mechanical analysis of traditional in-service glass windows subjected to dynamic tests and hard body impact

Lucia Figuli*[1,2], Daniel Papan [1,2b], Zuzana Papanova [1,2c] and Chiara Bedon [3d]

[1] *University of Žilina, Faculty of Security Engineering, Univerzitná 8215/1, 01026 Žilina, Slovakia*
[2] *University of Žilina, Faculty of Civil Engineering, Univerzitná 8215/1, 01026 Žilina, Slovakia*
[3] *University of Trieste, Department of Engineering and Architecture, Piazzale Europa 1, 34127 Trieste, Italy*

(*Received June 6, 2020, Revised September 22, 2020, Accepted October 6, 2020*)

Abstract. The large use of glass in buildings, and especially the presence of fenestrations and facade systems, represents a potential critical issue for people safety. The brittle nature of glass (with limited elastic deformation and resistance) is often enforced by its use in combination of several secondary components, whose reciprocal interaction and potential damage should be properly assessed. In the case of windows, accordingly, a special care should be spent for glass members but also for the framing system and possible adhesive or mechanical connections. This study aims at exploring the dynamic response and damage sensitivity of traditional glass window systems, based on the experimental derivation of few key material properties and mechanical parameters. To this aim the attention is focused on traditional, in-service windows that belongs to existing residential buildings and are typically sustained by timber frames, through a linear flexible connection. In doing so, major advantage is taken from experimental analysis, both in the static and dynamic field, for whole window assemblies of single components. For comparative purposes, selected window specimens including plastic (PVC) frame members and Insulated Glass Units (IGUs) are also taken into account in the paper. The static characteristics of the windows components are first preliminary derived. The dynamic performance of such a kind of systems is then experimentally explored with the support of modal analysis techniques and hard body impact procedures, including the experimental derivation of stiffness parameters for the frame members and the glass panels. Further assessment of experimental outcomes is finally achieved with the support of Finite Element numerical analyses.

Keywords: damage detection; glass; traditional in-service windows; experiments; modal analysis; hard body impact

1. Introduction

Glass is commonly used for cladding systems and facades. Among other design issues that still require research efforts, various motivations suggest the investigation of the dynamic response of glass systems under impact. Such a need is strictly related to the intrinsic vulnerability and fragility of these systems, see Bedon *et al.* (2018).

Most of the literature studies on glass under impact, however, are specifically focused on automobilistic or electronic applications, and limited efforts can be found for glass systems that are typical of civil engineering constructions. In this regard, experiments on laminated glass panels under the hard body impact (i.e., reproducing the effect of pedestrians or driver heads) have been carried out by Wang *et al.* (2018). Deformation and damage mechanisms of laminated glass windows when subjected to high velocity soft impact caused by bird strike were analyzed by Mohagheghian (Mohagheghian *et al.* 2017). Additional impact experiments are reported by Xue *et al.* (2013), and used to estimate the resistance of glass against scratches, drop impact and bumps. The reference configuration object of investigation, however, were properly chosen to describe the typical solution for the protection of displays for electronic devices (i.e., smartphones, tablets, etc.).

As far as load-bearing constructional systems are taken into account, even less literature studies can be found for glass structures under impact. Full-scale glass columns have been investigated by Bedon *et al.* (2017), under soft or hard body impact. In (Figuli *et al.* 2017, Figuli 2019), experiments for the burglary resistance and protection of glass "soft targets" are reported, together with some preliminary dynamic considerations for the behavioural characterization of glass windows under shock. An analysis of potential procedures for retrofit design was summarized by Bedon and Figuli (2017). Kruszka and Rekucki (2020) in their amply research conducting tests of the resistance of the window structure to soft impact a as well as to explosion.

Deformation and damage mechanisms of laminated glass windows subjected to high velocity soft impact caused by bird strike were analyzed by Mohagheghian *et al* (2017). A glass plate subjected to impact at different loading rates

*Corresponding author, Ph.D.,
E-mail: lucia.figuli@fbi.uniza.sk
[a] Ph.D., E-mail: daniel.papan@fstav.uniza.sk
[b] Ph.D., E-mail: zuzana.papanova@fstav.uniza.sk
[c] Assistant Professor, E-mail: chiara.bedon@dia.units.it

http://www.techno-press.org/?journal=sss&subpage=7
ISSN: 1738-1584 (Print), 1738-1991 (Online)

was analyzed by Bouzida (Bouzida *et al*. 2001) using two methods: the compression split Hopkinson pressure bar and the normalized ball drop test. A failure criterion for laminated glass in case of impact was earlier presented by Pyttel (Pyttel *et al*. 2011). Later on, symmetric plate-impact tests of borosilicate glass projectiles into borosilicate glass targets were performed by Chocron *et al*. (2016).

Compared to past literature efforts, the aim of this research paper is to analyze the prevailing load-bearing performance and damage mechanism (and thus vulnerability) of in-service glass windows under impact. The attention is focused on traditional glass windows of typical use in existing residential buildings, where timber framed systems are commonly used to brace simple monolithic glass panels, with linear flexible connections. Based on several experimental investigations at the component and assembly levels, both in the static and dynamic regime, some mechanical features are first assessed for the systems object of study. Successively, their hard body impact resistance is further explored. For comparative purposes, the selected traditional timber-glass windows are compared to modern, ordinary window systems, where plastic frame members are used in place of the timber members, as well as composite Insulated Glass Units (IGUs) replace the monolithic glass panels, with enhanced insulation benefits but also a mostly different mechanical behaviour (Bedon and Amadio 2020). The analysis of major experimental findings is finally enforced by Finite Element (FE) numerical simulations carried out in ABAQUS (Simulia 2020). As shown, the use of geometrically simplified numerical models for simple composite glass windows can represent an efficient tool in support of design and vulnerability analyses. Otherwise, the mechanical characterization of all the system components (including the secondary connections and materials at the glass-to-frame interface) has a crucial role. In this paper, based on inverse analysis procedures, the actual flexibility of the glass edge connections is numerically derived, and used as a reference for the dynamic investigation of the same specimens under impact. As shown, based on experimental feedback, the simplified FE modelling approach is found to offer a rather good correlation with the available impact test results.

2. Experimental analysis of glass windows

2.1 Specimens

Special care was spent to assess the sensitivity of the impact response of traditional in-service windows, as a function of the stiffness of glass and the mechanical features of the supporting frame, with respect to modern window solutions that can be used for ordinary residential buildings.

As known, the glass panels themselves represent the most vulnerable component for windows under impact, and envelopes in general. Besides that, further geometrical and mechanical aspect should be properly taken into account to describe their composite action, namely the supporting frame (if any) and the connections (adhesive, mechanical or hybrid) in use.

To this aim, each window sample was characterized by a total size A×B, including the net surface of the monolithic (annealed) glass plates and a continuous frame. Two window prototypes with global dimensions (A×B) were taken into account in the experimental investigation.

In the first case (SW-T), the chosen frame was made of timber, and reflecting the use in Czechoslovakia for residential buildings and offices over 1960s (Figs. 1(a)-(d)). The quantitative comparison of the experimental estimates was carried out towards a window specimen representative of a modern solution for ordinary windows (SW-P), thus including a plastic (PVC) frame of new construction, see Fig. 2.

From a mechanical point of view, the selected window specimens were characterized by marked variations in geometrical features and material properties.

For the research study herein summarized, the SW-T specimens were specifically disassembled from a real residential building. In this regard, the experimental analysis accounted for possible degradation phenomena for the in-service windows. According to Fig. 1(b), the typical SW-T window was characterized by A = 1.21 × B = 1.38 m dimensions, and included three timber framed systems. One of them is usually rigidly fixed to the building, while two movable frames are usually connected to the first one with small metal hinges (along the vertical edge). In both the

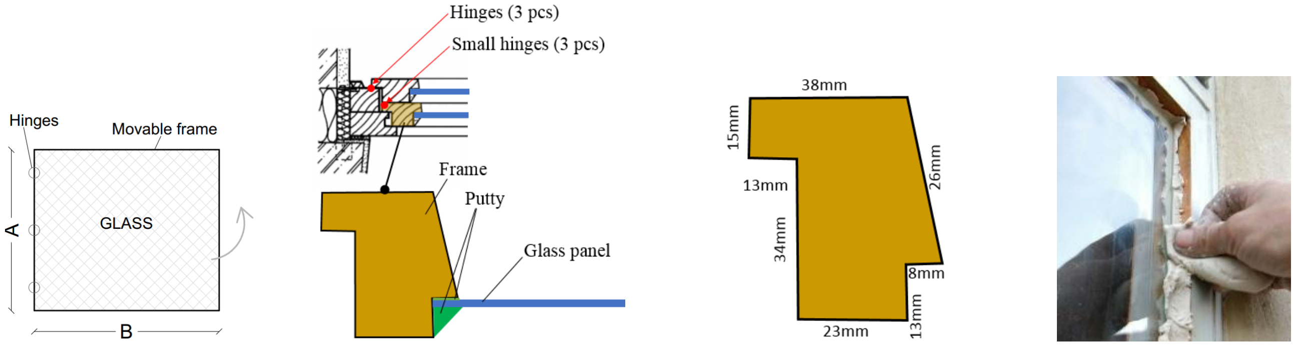

(a) Front view (b) Schematic cross-section of the system (c) Nominal dimensions of the movable timber frame members (d) Typical edge connection

Fig. 1 Preliminary visual inspection and measurement of the geometrical features for the traditional SW-T specimens object of study

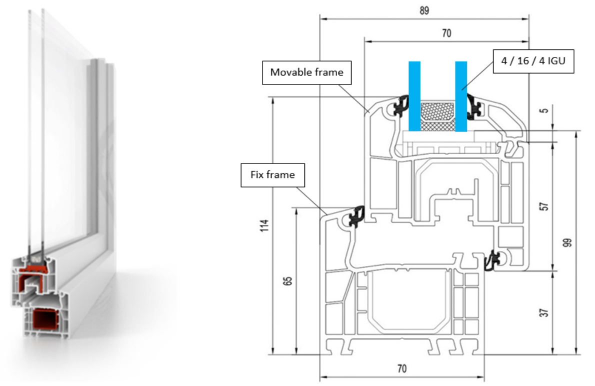

(a) Layout (b) Cross-section (dimensions in mm)

Fig. 2 Frame detail for the SW-P specimens

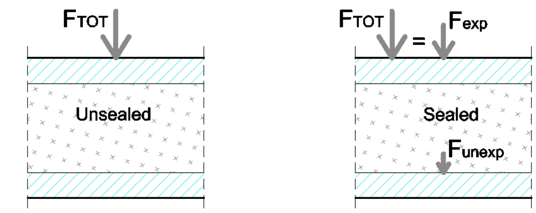

(a) Unsealed cavity (SW-T windows) (b) Hermetically sealed IGUs (SW-P windows)

Fig. 3 Qualitative mechanical response of double glass panels and expected distribution of external loads

movable parts, for the traditional windows herein explored, a 3 mm thick monolithic glass panel was used as infill. Fig. 1(c) shows the nominal cross-section for the reference movable frame members. Each glass panel, more in detail, was linearly connected to the corresponding frame system through a continuous layer of white, silicone-based gasket seal (putty), as in use at the time of the installation of the traditional windows (see Figs. 1(b) and (d)). At the preliminary stage of the experimental investigation, a visual inspection was carried out for confirmation. Nominal properties for these seals are in the range of ≈3.3MPa for the Modulus of Elasticity (MoE) and ≈ 5.8 MPa the tensile resistance (Arexons® SEAL 5661). Besides that, the tested window specimens included the effects of ageing and thus additional uncertainties on the actual mechanical properties of the sealant joints.

Given the presence of two movable glass-infilled timber frames, the cross-section of window under impact was characterized by the presence of a double monolithic section with an interposed (unsealed) air cavity. The lack of any sealing component for the cavity itself, in this regard, was not associated to a real IGU, thus the dynamic response of the SW-T specimens was physically focused to the assessment of an independent, timber frame supported monolithic glass plate with a mostly adhesive linear connection.

This is not the case of the SW-P specimens that were characterized by the reference cross-section in Fig. 2. The IDEAL-400 plastic frame from Aluplast® was used (Aluplast 2020). In this latter case, the movable frame was still hinged to the fix components of the window assembly. On the other side, the typical resisting cross-section was characterized by the presence of a double IGU with two 4mm thick annealed glass panels and an interposed, 16mm thick cavity, thus including the well-known “load sharing phenomena”, as well as additional mechanical effects due to the edge spacer connection in use (Bedon and Amadio 2020).

2.2 Experimental methods

To assess the mechanical response and the damage sensitivity of glass windows to hard body impact, a series of experimental measurements were conducted based on different testing approaches.

Given that the SW-T and SW-P frames were characterized by some trivial geometrical variations, the net surface of glass, A_{glass}, was deducted from the A×B total area deprived of the frame members. As a result, the exposed surface of glass resulted in

$$A_{glass} = A_g \times B_g = \{1.20 \times 1.05 = 1.26\, m^2 \text{ for } SW - T\ 0.81 \times 0.97 = 0.786\, m^2 \text{ for } SW - P \tag{1}$$

respectively. Another relevant difference was represented by the nominal thickness of glass, that was set in 3 mm (independent) and 4 mm (IGU) for the SW-T and SW-P specimens respectively.

For a unit of length of cross-section, their qualitative mechanical behaviour against the imposed design loads agrees with the schematic drawing of Fig. 3. The same composite IGU effect is even further enforced by several other details (type and size of the frame, glass thickness and size, edge spacer connections for IGUs, etc.).

From a bending stiffness consideration, finally, the schematic drawings of Fig. 3 can roughly suggest that the independent glass panel is expected to sustain the imposed loads with an ideal out-of-plane bending rigidity equal to

$$D = \frac{Eh^3}{12(1-\nu^2)} \tag{2}$$

with h = 3 mm the glass thickness (E and ν the properties of glass). In the case of Fig. 3(b), otherwise, the same bending stiffness contribution could ideally tend (at the upmost) towards the sum of the bending contributions of both the glass panels (with h = 4 mm), thus resulting in a potential +127% increase of the rigidity per unit of length for the SW-P specimens, compared to the SW-T windows.

Besides that, the actual mechanical contribution for all the involved load-bearing components should be properly assessed, case by case. This is especially the case of the supporting frames (that are expected to offer a certain bracing system to glass, through linear connections at the glass edges) and the overall bending behavior of the so assembled glass-framed systems.

To this aim, accordingly, the experimental investigation on the examined window prototypes included a preliminary stage with:

- static bending experiments (on a single movable framed window only), along with

- static bending experiments for timber members and glass specimens (for the SW-T windows only),
- non-destructive dynamic experiments (on a single movable framed window only),
- impact dynamic experiments (on the overall window system), based on the ball drop test setup.

Given the input features described in Section 2.1, the single movable framed specimen for SW-T or SW-P specimens was respectively inclusive of:

- a single monolithic, 3 mm thick glass panel agreeing with Fig. 1, or
- an IGU panel (4/16/4) with geometrical features in Fig. 2.

3. Discussion of preliminary experiments

3.1 Static bending experiments

The typical test was carried out in accordance with Fig. 4. The specimen was positioned on four steel supports at the corners, and thus loaded at the center, via the testing apparatus. A monotonic vertical load F was imposed at the centre of the window, while monitoring the corresponding deflection u by means of a Sylvac digital deflection gauge (Papán and Papánová 2020).

The static experiments on the SW-T sample included two loading stages. First, see Fig. 5(a), the specimen was loaded and unloaded in the elastic range, i.e., up to a total displacement u = 8 mm (with F = 35 N the corresponding imposed load). A rather stable bending response was observed in the loading-unloading stage. Successively, the specimen was reloaded up to failure, that was achieved for a total imposed load F = 95 N and a corresponding middle deflection u = 13.5 mm. The collapse mechanism of the SW-T specimen, given the annealed, monolithic glass section in use, was characterized by the abrupt propagation of large shards, with null residual capacity of the window see Fig. 5(b).

In terms of static bending response, moreover, the SW-T specimen proved to offer a relatively weak rigidity compared to the SW-P sample. From Fig. 5(a), the average bending stiffness of the SW-T specimen was measured in K_{bend} = 1.78 N/mm (secant stiffness value), while for the SW-P specimen under an identical imposed loading ratio F, the bending stiffness was predicted in K_{bend} = 2.83 N/mm (+58.9%). Such a finding can be rationally justified both by the glass section in use (3mm monolithic panel, in place of a sandwich 4/16/4 IGU panel), as well as by the frame properties (timber or PVC sections, with specific inertial features). In Fig. 5(a), this effect can be perceived from the load-deflection responses that are proposed is shown for comparative purposes.

A special attention was spent successively for the timber frame members, given that they actually represent a continuous bracing system for the glass panels. Accordingly, the glass panel itself is expected to offer a plate bending stiffness to the window, based on the thickness in use (3 mm the nominal value) and the MoE of glass.

In this regard, after the bending experiments on whole window specimens, the attention was focused on the static bending analysis of window components, namely the timber frame members and the glass plate. Fig. 6 gives evidence of the additional experimental measurements. For the timber members, see Fig. 6(a), these were obtained from the destructive bending test on the composite window earlier investigated. Accordingly, some big glass shards were collected and separately assessed, via the conventional 3-point bending test setup see Fig. 6(b). From such a series of experimental records, the static longitudinal MoE of timber was predicted in a mean E_{long} = 9.2 GPa value. For glass characterization, the attention of the experiments was dedicated on selected large shards only, that were

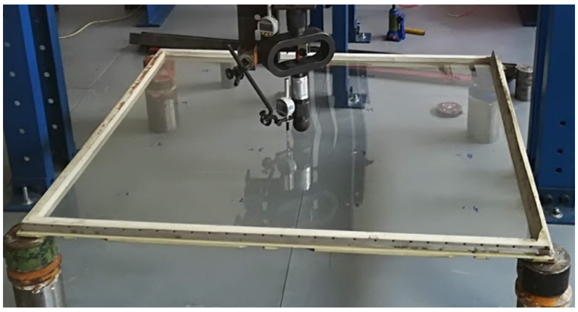

Fig. 4 Static bending experiments on movable framed windows (SW-T specimen)

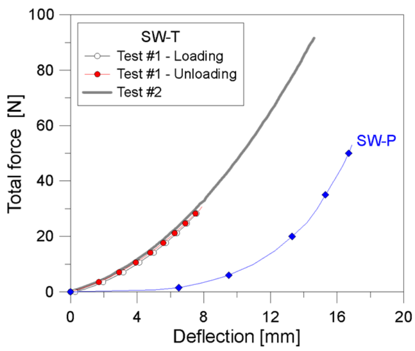

(a) Measured load-deflection response

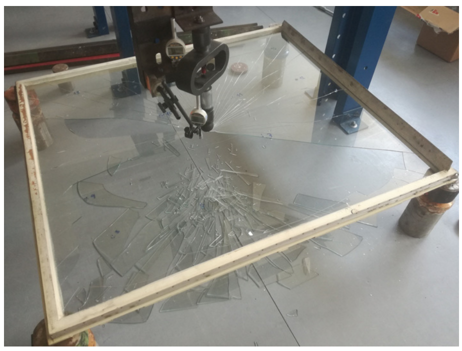

(b) Collapse configuration

Fig. 5 Static experiments on the SW-T specimen (movable framed window)

(a) Timber frame (b) Glass

Fig. 6 Static bending experiments on movable framed windows (SW-T specimen)

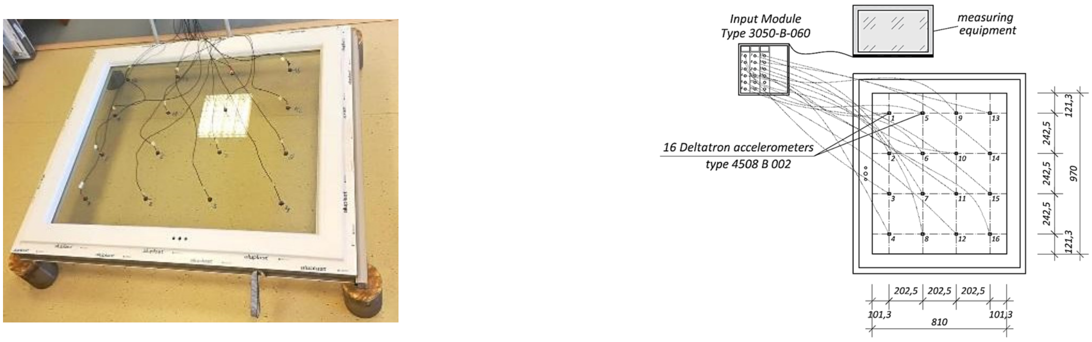

(a) Specimen and supports (b) Layout of the instruments in use (with nominal dimensions in mm)

Fig. 7 Experimental modal analysis of the SW-P plastic window

characterized by 3 mm in thickness and 30-40 mm in width, with ≈ 15-20 the average length-to-width ratio. The mean MoE of annealed glass was calculated from four glass shard specimens in bending agreeing with Fig. 6(b), and resulting in an average experimental measurement of E_{glass} = 67.8 GPa.

3.2 Non-destructive dynamic experiments

The second stage of experimental studies included a series of non-destructive dynamic measurements on the integer SW-T and SW-P window prototypes. Modal dynamic analyses were in fact carried out, before the destructive impact tests, in order to further assess the fundamental vibration frequency and modal shape for the examined windows.

The typical specimen is shown in Fig. 7(a), while Fig. 7(b) presents a schematic layout of the instruments in use. A rectangular grid with 16 Deltatron accelerometers (type 4508 B 002) was installed evenly on the glass surface. Three six channels input modules (Type 3050-B-060) were used for the acquisition of data. Each accelerometer was then cable-connected to an Input Module (with two inactive positions). The measuring interfaces were thus connected to a PC, so that the test records could be processed via the PULSE software.

To this aim, the window specimens were supported on steel devices at the corners, so as to reproduce the same boundary conditions of the static experiments described in Section 3.1. The imposed excitation was realized by tapping the glass windows with various levels of impact softness, at the middle grid points of the glass surface. The measured data were then transformed into the ARTeMIS software. In Table 1, the so-calculated fundamental frequencies and modal shapes are proposed, for both the SW-T and SW-P specimens.

From the interpretation of the modal experimental measurements, see Table 1, some important aspects were observed on the overall dynamics of the investigated specimens. For the SW-T window, the monolithic glass panel can be in fact regarded as a thin plate with a continuous, flexible bracing frame along the edges. In the case of the SW-P specimen, the sandwich IGU panel is still responsible of a composite bending action for the two 4mm glass layers in use (Fig. 3). The latter, moreover, is further enforced by the PVC bracing frame, thus resulting in relatively higher rigidity and bending stiffness as a whole, with obvious load bearing benefits for the single glass members.

For the reference boundary condition in Fig. 7(a) with ideal pin-supported corners, major effects due to geometrical and mechanical features for the SW-T and SW-P specimens can be perceived for the fundamental modal shape in Table 1, as well as for higher vibration modes. While the lowest modal shape for both the windows typologies of Table 1 still agrees with the global bending deformation of a pin supported plate, the calculated frequency is indeed in the range of ≈ 13 Hz and ≈ 21 Hz respectively (+61.5%). Such a frequency scatter, as shown, is in close correlation with the static bending estimates, where the SW-P window proved to offer a bending increase in the order of +58.9%, with respect to the SW-T specimen.

Table 1 Experimental modal analysis – Vibration frequencies and modes

Mode order	SW-T window	SW-P window
1	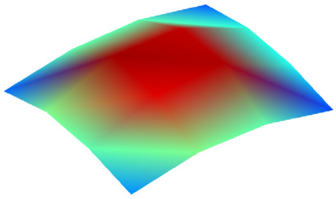 $f_1 = 13.1$ Hz	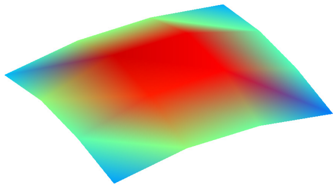 $f_1 = 21.03$ Hz
2	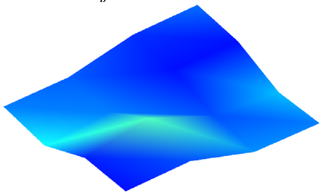 $f_2 = 51.26$ Hz	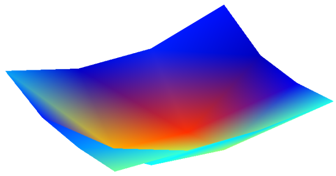 $f_2 = 48.36$ Hz
3	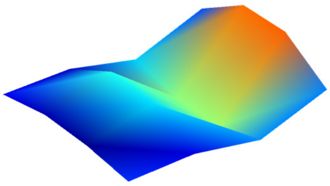 $f_3 = 63.75$ Hz	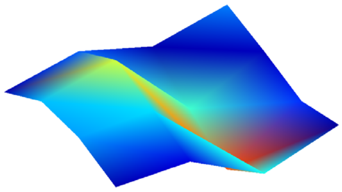 $f_3 = 71.56$ Hz
4	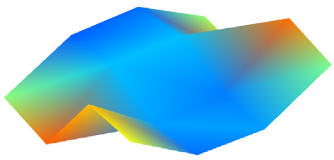 $f_4 = 76.75$ Hz	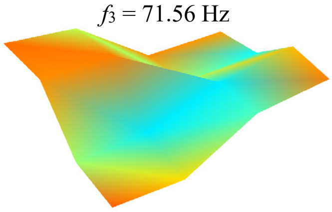 $f_4 = 81.53$ Hz
5	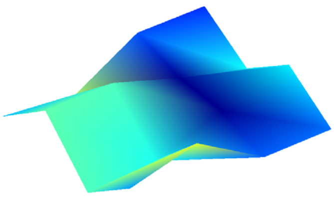 $f_5 = 122.2$ Hz	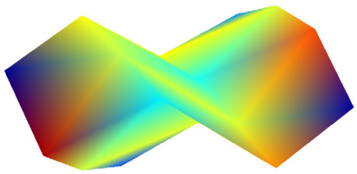 $f_5 = 158$ Hz

3.3 Finite Element frequency analysis

In order to further explore the overall performance of the testes SW-T windows, a series of FE numerical analyses was successively carried out in ABAQUS. In doing so, to reproduce the movable framed system earlier tested, a set of beam (B31) and shell (S4R) elements were used, and properly combined through a series of springs.

In the case of the timber frame, more in detail, the nominal movable cross-section in Fig. 1 was schematized as described in Fig. 8(a). Accordingly, monolithic shell elements were used to account for the glass panel. Based on the nominal geometry of the tested SW-T windows, as well as on the geometrical approximations induced by the beam-shell FE model in use, a section offset was assigned to the glass shell elements (Fig. 1(a)).

A special role was thus assigned to a series of springs that were used to allow the mechanical interaction of the timber frame members and the glass plate. To this aim, more in detail, the input stiffness parameters were derived from preliminary calculations and comparative fitting with the corresponding experimental estimates for the same SW-T windows. Based on the knowledge of the nominal dimensions and MoE values both for timber and for glass, the major uncertainty was in fact represented by their putty linear connection. Such an issue derived both from the lack of detailed feedback on the materials in use at the time of the installation of the buildings, as well as from the uncertainty on the durability of the same edge connections, given that the tested windows were disassembled from a real residential building.

Accordingly, a parametric FE investigation was carried out on the so assembled FE model, so as to explore the effects on frequency and static bending estimates for the so assembled timber-glass composite system.

Regarding the vibration performance of the SW-T windows, selected FE results are proposed in Figs. 8(b) and (c), where the fundamental modal shape and the sensitivity of the FE fundamental frequency are proposed. By varying the equivalent stiffness for the layer of springs in use, the

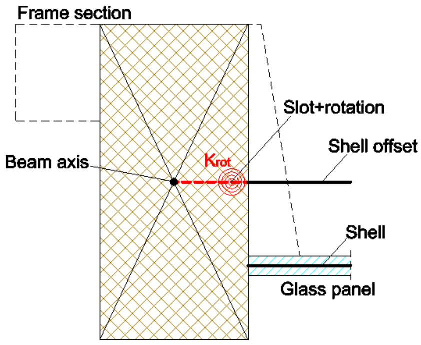

(a) Modelling detail

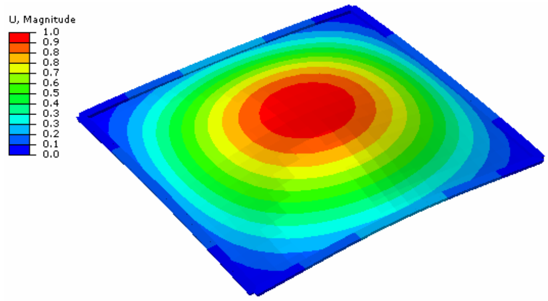

(b) Fundamental vibration shape

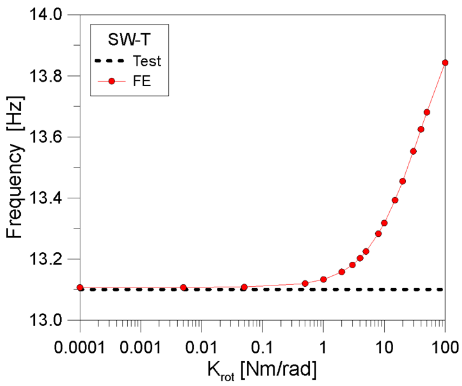

(c) Vibration frequency, as a function of the rotational stiffness of the edge connection

Fig. 8 Numerical frequency analysis for the SW-T window specimen (ABAQUS)

vibration frequency of the pin-supported SW-T window was found to suffer for major variations, compared to the experimental prediction. Moreover, the experimental fitting of the fundamental frequency resulted in a relatively weak rotational connection between the glass plate and the timber frame (Fig. 8(c)). This outcome is in close correlation with earlier studies on the vibrational analysis of simple glass elements (see Bedon *et al*. 2019), where it was proved that the soft layers and gaskets that are typically use in boundaries and restraints for structural glass applications (to avoid premature stress peaks) are commonly associated to an intrinsic additional flexibility of supports, that should be properly taken into account for design considerations, in place of ideally rigid restraints. In this specific research study, such a finding was further enforced by the presence of a putty layer including the effects of degradation due to ageing and long-term phenomena, for a relatively weak and brittle in tension material.

Most of the attention was focused on the fundamental vibration mode of the window, given that it represents the prevailing bending mechanism for the examined specimens under the imposed impact. Besides that, the use of geometrically simplified FE assemblies for glass composite systems should be generally calibrated and supported by experimental data and / or analytical studies, given that a multitude of parameters of primary interest (i.e., frame details, glass properties, connections, boundaries, etc.) can have a relevant role on the overall structural response analysis. In this specific study, for example, it is important to further remind the effect of boundary conditions, given that the preliminary experimental study was carried out in laboratory conditions that do not represent the final mechanical configuration for the investigated windows.

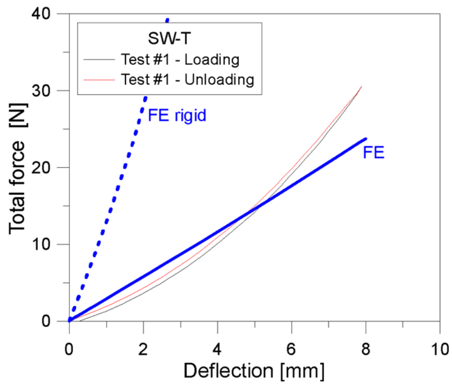

Fig. 9 Numerical analysis of the bending response of the SW-T specimen under a maximum imposed deflection of 8mm at the centre of glass (ABAQUS). In evidence, the effect of spring connections between the glass panel and the timber frame

Regarding the static bending performance of the same SW-T specimen, see Fig. 9, the same modelling approach (even roughly simplified) resulted in a rather good estimate of the load-deflection response from the experimental study. In the latter case, non-linear static numerical analyses were carried out for the pin-supported FE model of the window, by imposing a monotonic load at the centre of glass, in order to reproduce the test setup in Fig. 4.

Worth of interest in Fig. 9 is that the “FE rigid” plot (i.e., that assumes a fully rigid connection between the pin-supported elastic frame and the glass plate) is highly overestimating the actual bending stiffness of the window, thus enforcing the critical role of soft layers and weak connections that are of typical use for glass applications.

4. Hard body impact experiments

4.1 Setup and methods

Later on, a series of hard body impact experiments were performed on the selected windows, based on a reference test setup agreeing with Fig. 10. The typical impact test was organized in accordance with the standard pendulum testing procedure. The impactor consisted, as in the case of conventional ball drop test procedures, in a steel ball with given diameter and weight. To this aim, a rigid metal frame was used to restraint the window specimens in a vertical position. This choice resulted in linearly clamped transoms for the frame systems. Moreover, the setup was arranged so that the steel ball could impact the target window in the center of glass panel. For both the SW-T and SW-P specimens, the whole window systems were experimentally investigated under impact. As such, the impact body resulted in a fully independent, 3 mm thick monolithic section for the SW-T window (Fig. 3(a)), and in a 4/16/4 composite IGU panel for the SW-P specimen (Fig. 3(b)).

Two different impact bodies were used during the overall experimental campaign, namely represented by steel balls with a nominal weight of m = 2.644 kg or m = 4.571 kg respectively. The length of the pendulum in Fig. 10(a) was kept fix (L = 2.56 m) for the whole experimental program. On the other side, variations were accounted for the drop height (and thus on the horizontal distance d between the ball and the window).

In each test, the acceleration of the impacted window specimens was thus measured by means of an accelerometer, that was positioned in the lower corner of the glass panel (i.e., on the right side of the specimens, at a distance of 0.2 m from the lateral and bottom edges, see Fig. 11(b)). In this manner, any possible trouble in the instruments in use (due to the impacting ball and the propagation of cracks in glass) was minimized. Finally, a high-speed camera (FASTEC TS3100SC4256 Imaging) was also used in combination with the accelerometers, in order to investigate the velocity of the system based on slow motion video registrations.

Four test investigations (#1-to-#4, in the following) were carried out on the SW-T or SW-P window specimens, by changing the size of the steel ball (mass m) and the drop height / distance d from the glass surface (and thus the imposed overall impact energy E_{impact}). This height was

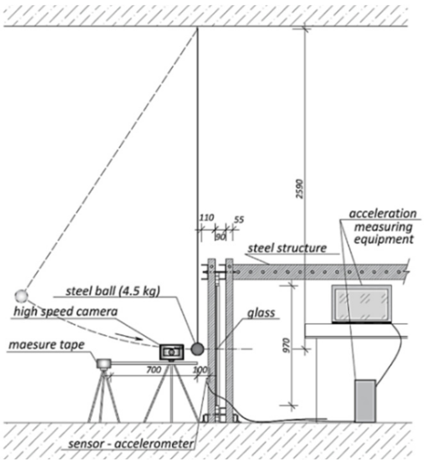

(a) Schematic drawing of the reference setup (side view, with nominal dimensions in mm)

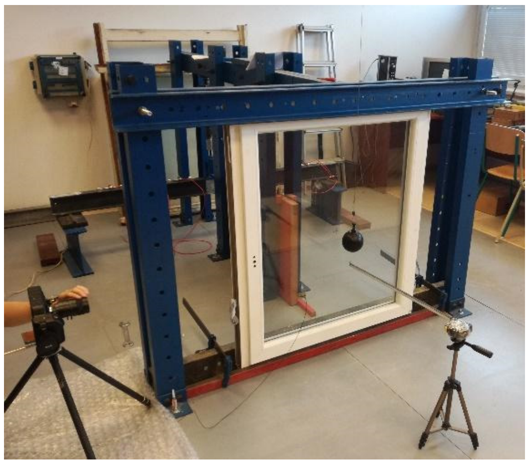
(b) Laboratory test setup and instruments

Fig. 10 Hard body impact experiments

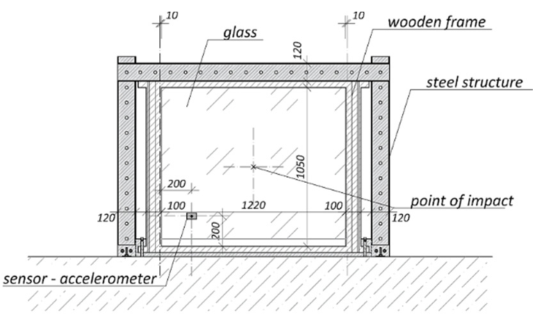

(a) ST-W

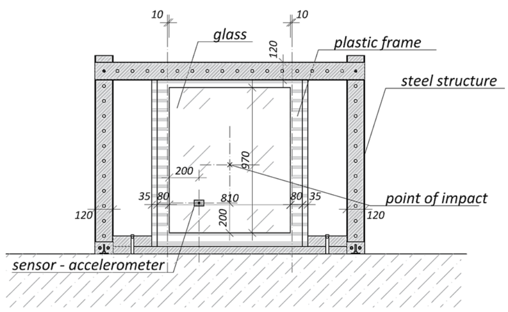

(b) ST-P specimens (with nominal dimensions in mm)

Fig. 11 Front view of the experimental setup progressively increased, so as to lead the glass panels to failure ($E_{impact} = E_{failure}$). The same energy was calculated, for each test repetition, by taking advantage of slow motion records of the high-speed camera. By taking advantage of the accelerometer in use, the out-of-plane (horizontal) acceleration and velocity peaks a_{max}, v_{max} were also derived for the specimens.

While progressively increasing the imposed impact energy, any possible damage in the glass panels was also visually inspected. This monitoring step was facilitated by the use of monolithic annealed glass panels that are typically associated to large and visible (and thus dangerous) shards.

4.2 Analysis of experimental results

4.2.1 Elastic response

An example of the typical acceleration records is proposed in Fig. 12, for two selected SW-T and SW-P specimens under low / medium impact configurations (with m = 2.644 kg). For both of them, the dynamic response was classified as fully linear elastic, given that no visible damage was observed neither in the annealed glass panels nor in the frame members.

As far as acceleration trend of Fig. 12 is taken into account, in particular, some important considerations can be derived on the impact behaviour of the window in the elastic regime. At a first sight, for example, the SW-P specimens proved to offer an enhanced stiffness and resistance to impact loads, compared to the SW-T windows.

More in detail, based on Fig. 12(a), the damping capacity of the SW-T windows was experimentally derived from the recorded data. A mean value in the order of ξ_{TOT} = 20% was roughly calculated from Fig. 12(a), being inclusive of structural damping, aeroelastic damping, and damping due to progressive damage (if any), that is

$$\xi_{TOT} = \xi_{struct} + \xi_{aer}(+\xi_{dam}) \tag{3}$$

In the case of glass elements, in this regard, material damping effects are known to be limited (i.e., in the order of ξ_{struct} = 1-2%, especially for monolithic glass deprived of the interlayer foils, see Bedon *et al*. 2019. Moreover, no visible damage was visually detected for most of the experimental configurations (with the exception of the last test for each series, where the glass panels were lead to collapse), hence $\xi_{dam} = 0$ in Eq. (3).

Finally, the aeroelastic damping contribution ξ_{aer} of a given SW-T window under impact could be analytically estimated on the base of a simplified analytical model for the moving specimen, so as to have at least a first quantitative assessment of the specimen response. Assuming that the whole glass surface vibrates under the imposed impacting ball with its own fundamental frequency, in particular, it was found by Bedon and Amadio 2014, that possible aeroelastic phenomena can be calculated as

$$\xi_{aer} = \frac{c_d \rho_{air} S_{glass} v_{max}}{2 M_{TOT} \varpi_1} \tag{4}$$

In Eq. (4), c_d = 1 represents the drag coefficient, ρ_{air} = 1.225 kg/m^3 the density of air, S_{glass} and M_{TOT} the total moving surface and mass respectively. Finally, v_{max} represents the maximum velocity of the window under impact-induced vibrations, with a natural fundamental pulsation ω_1. Based on the actual modal parameters of the examined SW-T specimens, it is worth of interest that the impact configuration reported in Fig. 12(a) would result in

$$\xi_{TOT} = 2 + 17.75 = 19.75\% \approx 20\% \tag{5}$$

that closely matches the exponential decay fitting of test records.

Besides such a finding, however, maximum effects in the window components under impact cannot take advantage of the above damping contributions. This is especially the case of maximum tensile stresses in glass. The latter should be checked both in the region of impact as well as in the vicinity of the supporting systems (if any, due to the effects of local stiffness). Accordingly, Eqs. (3)-(5) could represent a useful support for enhanced calculations only, as far as the windows object of analysis are still verified against the stress peaks due to the assigned shock loads.

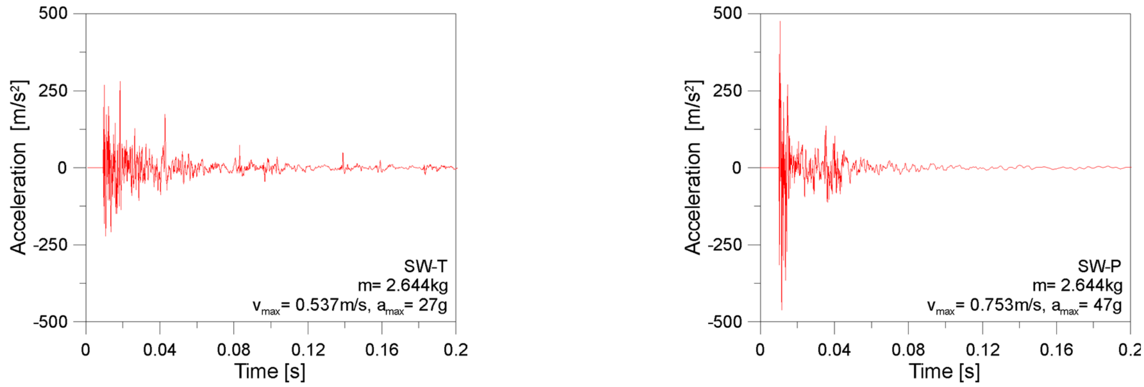

(a) SW-T (b) SW-P

Fig. 12 Example of recorded acceleration time histories for window specimens with fully elastic response (from control point in Fig. 11(b))

(a) SW-T

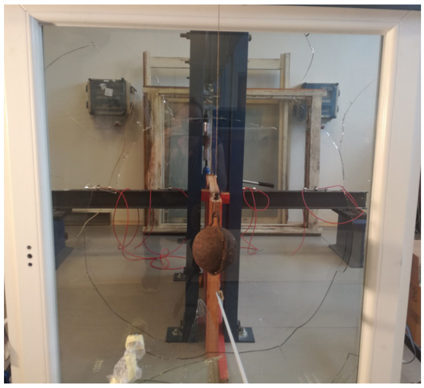

(b) SW-P specimens at collapse

Fig. 13 Example of failure mechanism

4.2.2 Collapse mechanism

As far as the impact energy was increased in the setup of Fig. 10(a) until failure of the tested windows, the typical experimental collapse mechanism was characterized by the crack pattern shown in Fig. 13. Failure occurred due to a sudden and irreversible cracking mechanism that (propagating from the region of impact) generally spread towards the edges of glass panels. The typical size and shape of annealed glass shards can be also perceived from Fig. 13.

More in detail, the post-processing stage was focused on the time of failure of glass, and on the calculation of the ball velocity $v_{failure}$ recorded at the occurrence of damage. Given that annealed monolithic glass panels were used for the examined specimens, damage was always associated to the propagation of severe cracks in glass, that were easily detected by visual inspection of the windows. Accordingly, no residual capacity was observed for them. Based on the experimentally measured values of the velocity peak for the ball ($v_{failure}$), the corresponding impact energy at collapse was hence estimated as

$$E_{failure} = \frac{1}{2} m\, v_{failure}^2 \tag{6}$$

Some relevant experimental parameters are presented in Table 2 for each window specimen at collapse, as a function of the ball size, the level of impact energy and the measured final velocity of glass (control point).

For three SW-T specimens, the experimental data collected in Table 2 show a rather stable impact resistance for the specimens #1 and #3. This is suggested by the maximum impact velocity of the ball, that was sustained in the range of ≈ 2.5 m/s, with a mean corresponding energy of ≈ 8.3 J. The corresponding final velocity for the glass windows was experimentally measured in ≈ 0.3 m/s. For the specimen #2 with identical nominal features, on the other side, a premature collapse was observed for a velocity peak of 1.6 m/s and an impact energy of 3.36 J (with 0.2 m/s the corresponding final velocity for the glass window), thus denoting less than half the impact resistance of specimens #1 and #3. Such a finding could be first justified by the possible occurrence of progressive degradation phenomena for the tested traditional in-service windows (i.e., weak connections, defects, etc.), and thus a corrupted mechanical response of the specimen. Moreover, this experimental observation finds explanation especially in the typically scattered tensile resistance of annealed glass, that is known to suffer for strong variations, compared to the nominal characteristic value and to the occurrence of high strain rate phenomena (with 45 MPa for annealed glass in static conditions (EN 572–2:2004)). The limited number of test repetitions, however, does not allow to derive generalized conclusions, but is intended to support the analysis and interpretation of local parameters, and their effects on the global dynamic observations.

Finally, it is worth of interest in Table 2 that the SW-P specimen was lead to collapse for a total imposed energy in the order of 19.75 J, that would correspond to a +135% of the overall resistance for the window specimen under impact, compared to the SW-T samples #1 and #3. The final

Table 2 Experimentally measured impact energy at failure for the SW-T and SW-P window specimens under various impact configurations, and corresponding final velocity for glass

Test	Specimen type	Ball mass	Ball distance	Impact velocity	Impact energy	Final window velocity
		m [kg]	d [m]	$v_{failure}$ [m/s]	$E_{failure}$ [J]	v_{glass} [m/s]
#1	SW-T	2.644	1.30	2.42	7.72	0.30
#2	SW-T	2.644	0.90	1.60	3.36	0.20
#3	SW-T	2.644	1.40	2.59	8.90	0.32
#4	SW-P	4.571	0.15	2.94	19.75	0.37

velocity of the SW-P specimen was measured in the order of 0.37 m/s. With respect to the static bending and modal measurements, where the SW-P response was previously estimated in a ≈ +60% of enhancement compared to the SW-T predictions, such a finding still confirms the marked variation of bending properties and overall capacity for the tested glass panels (i.e., Fig. 3), but also a rather complex combination of multiple influencing parameters (both related to the geometrical and mechanical features of the specimens, as well as to additional high strain rate phenomena) that should be separately assessed through additional, extensive experimental investigations.

4.2.3 Analysis of maximum effects due to steel ball impact

Based on the experimental outcomes earlier summarized, a final attempt was carried out with the support of FE numerical simulations. More in detail, the dynamic response of SW-T specimens under the steel ball impact setup was explored, by taking advantage of the reference FE assembly that was earlier calibrated for static bending experimental data an modal dynamic measurements.

The non-linear dynamic analysis was carried out in ABAQUS/Explicit (Simulia 2020), on FE models agreeing with Fig. 14(a). To this aim, the impact of the steel ball was properly taken into account with the support of experimental details, that is by imposing a given velocity to the impacting steel body and introducing appropriate contact interactions with the adjacent glass surface.

For comparative purposes, glass was still described in the form of a linear elastic material, with an input average MoE from the conducted static bending experiments. The boundary conditions of the frame members were properly adapted, so as to agree with the test setup in Fig. 10. The typical distribution of tensile stresses in glass was generally recorded in the region of impact, see Fig. 14(b). Besides that, a careful consideration was generally paid for the analysis and detection of possible stress peaks in the vicinity of the supporting frame. In this context, the linear flexible connection at the interface of glass and frame member was numerically described as previously discussed. Such an assumption was found, as in the case of static loading conditions, a crucial role on the collected dynamic predictions.

A set of parametric numerical analyses was in fact carried out on the FE model in Fig. 14(a), so as to explore the maximum expected effects on the glass window, under different impact configurations. In the numerical study, the position of the steel ball was kept fix and in the center of

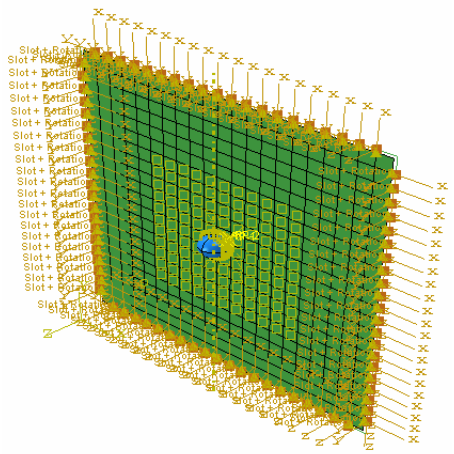

(a) Definition of impact loading

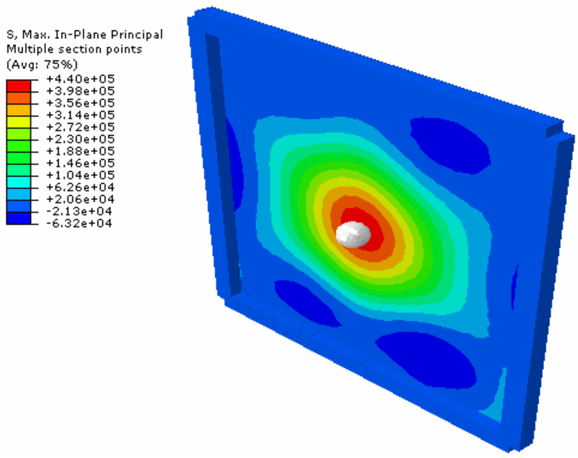

(b) Typical distribution of stresses in glass, at the time of impact (legend values in Pa)

Fig. 14 Reference FE model for the analysis of SW-T windows under the ball drop setup (ABAQUS)

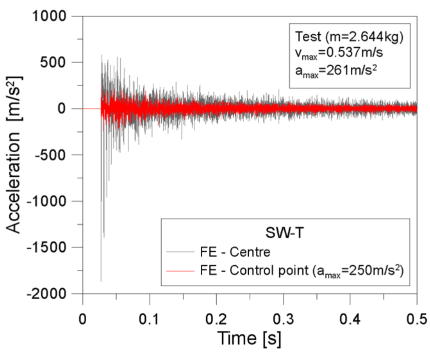

(a) Acceleration history

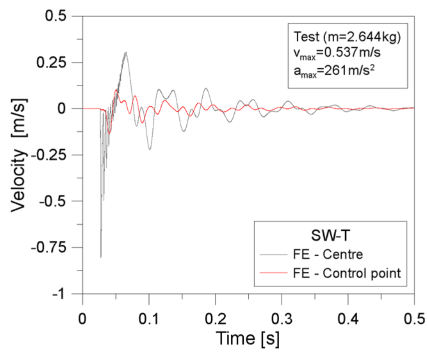

(b) Velocity history

Fig. 15 Numerical analysis of the SW-T window specimen with elastic response under hard body impact (ABAQUS) glass (i.e., as in the case of the full-scale experiments), while progressively increasing the imposed impact velocity for the steel ball. Its value was modified in the range from 0.1 m/s to a maximum of 3 m/s (based also on Table 2), with a total of ten intermediate values. In this manner, a special attention was dedicated to the dynamic response of the system, and specifically the evolution of the numerically measured velocity of the window (for comparisons with the v_{glass} experimental values), and the predicted tensile stress peaks in glass.

In Fig. 15, selected FE results are proposed for the SW-T specimen with elastic response (i.e., under a steel ball with v_{max} = 0.537 m/s of impact velocity). The attention is focused on measured accelerations (Fig. 15(a)) and velocities (Fig. 15(b)), both at the centre of glass or at the selected control point. For the second one, the numerical analysis reported in Fig. 15(a) shows a good correlation for the measured acceleration peak, with a_{max} = 261 m/s^2 and 250 m/s^2 from the laboratory test and the numerical model respectively. Besides, the FE results in Figs. 15(a) and (b) further emphasizes much severe maximum impact effects at the centre of glass, where no experimental instruments can be used for direct measurements. Regarding the overall dynamic response of the system, moreover, the developed FE model generally proved to capture very well the maximum expected peaks due to hard body impact. An example is shown in Fig. 16(a), where the final velocity values are proposed for the SW-T model under various impact configurations (m = 2.644 kg), and compared with the experimentally derived values for the specimens #1, #2 and #3 at collapse (Table 2). In the same figure, simple analytical estimates are also proposed for the same SW-T window specimens, as obtained in (Figuli *et al*. 2020) with the support of Single Degree of Freedom (SDOF) approximate calculations. The same SDOF approach reported in (Figuli *et al*. 2020), however, still gave evidence of major uncertainties in the reliable characterization of the examined window specimens, including stiffness parameters and boundaries.

Based on the available experimental outcomes, the parametric analysis of this study was mainly focused on the critical effects in the examined windows, rather than on the analysis of the whole dynamic response in time. This is also the case of the numerically predicted tensile stress peaks in glass (Fig. 16(b)), that can give further valuable feedback on the potential collapse of the system.

While the static bending tensile resistance of annealed float glass is in fact generally assumed in a mean characteristic value of 45 MPa (EN 572–2:2004), its nominal value is notoriously highly sensitive to the loading conditions of interest, both for long-term loads or even impact events. High strain rates, as in the current research study, are commonly associated to a dynamic amplification factor that can take the form of an enhanced tensile resistance value for glass. Limited test measurements are however available in the literature for glass under severe dynamic loads. Among others, Brown (1974) found for example that the dynamic tensile strength of annealed float glass can increase, thanks to the Dynamic Increment Factor (DIF), up to DIF ≈ 3 times (i.e., ≈ 135 MPa) its quasi-static nominal value in bending. According to past literature efforts on glass elements under blast and shock events, the recommended "effective" resistance value for annealed glass was thus defined in 84.8 MPa by Meyers (1994), corresponding to a DIF value of ≈ 1.87. In the SSG Glazing Hazard Guide (1997), the reference tensile resistance of annealed glass under shock was proposed in the order of 80 MPa (DIF ≈ 1.77).

A selection of FE parametric results is proposed in Fig. 16(b), with a focus on the measured stress peaks in glass. For all the examined configurations, the typical resisting mechanism was still found to agree with Fig. 14(b), with the exception of a progressive increase of mechanical effects in the load-bearing components, with the increase of the imposed ball velocity. As shown in Fig. 16(b), the stress peak evolution at the centre of the window was found to have a mostly linear trend, and to progressively increase with the impact magnitude, before that any dissipation phenomena could manifest. As far as the experimental collapse configurations in Table 2 are taken into account, it is possible to see that the experiments #1 and #3 roughly correspond to a dynamic tensile resistance of glass in the range of ≈ 98-105 MPa (with a calculated DIF ≈ 2.5), while the latter would be in the range of ≈ 65 MPa for the specimen #2 (thus in the order of DIF ≈ 1.4).

Certainly, the limited availability of three collapsed specimens only requires further extended investigations on similar windows. Besides, it is worth of interest that a mean experimental resistance of 89.3 MPa can be preliminary derived from the average failure configuration of specimens

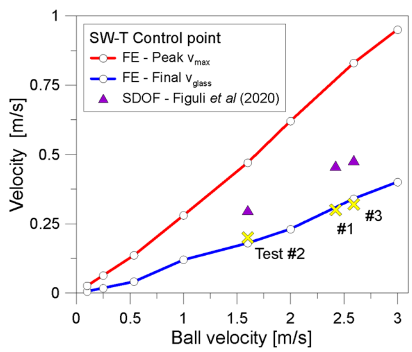

(a) Velocity

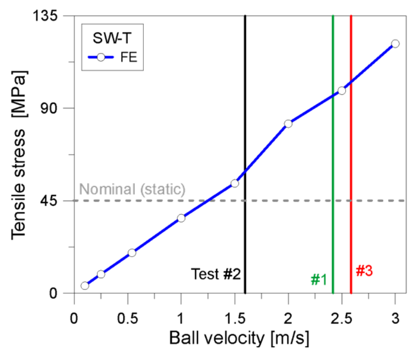

(b) Tensile stress

Fig. 16 Numerical analysis of the SW-T window specimen with elastic response under hard body impact (ABAQUS)

#1, #2, #3 (DIF ≈ 1.98), and the so-calculated value – even from early stage experiments only – is in close correlation with literature studies on annealed glass under shock events. The same average dynamic resistance, that is numerically fitted in 89.3 MPa, further remarks from Fig. 16(b) the high variability of the tensile resistance for glass, both under static and dynamic design loads. The mean numerical results still highlights a range of variability in the order of ≈ 40 MPa (in between ≈ 65 MPa and ≈ 105 MPa), thus enforcing the critical role of ordinary windows in buildings, and the need of dedicated interventions.

5. Conclusions

Due to the intrinsic material brittleness, glass windows are known to represent one of the most vulnerable building components, and thus require dedicated studies or retrofit interventions. This is especially the case of existing, in-service glass systems in traditional buildings, where the lack of appropriate safety rules and design methods can further enforce this implicit vulnerability, and thus the potential risk for injured people in case of accidental events. In this research paper, special care was spent for the analysis of traditional, in-service glass windows and for their experimental characterization, with the support of both static test procedures and dynamic approaches. Thanks to static bending experiments and modal analysis investigations, more in detail, the basic mechanical properties of window components were characterized in support of hard body impact experiments. In doing so, Finite Element (FE) numerical models were also developed, in order to offer a further insight on the actual mechanical interaction of simple window components.

As a reference, ordinary monolithic glass windows with bracing frame members made of timber were in fact explored, at the component as well as at the assembly levels. As far as the geometrical properties of ordinary windows are known, as shown in the paper, major uncertainties can lie on the actual material properties of glass (due to their high variability), but especially on the joints in use to provide the mechanical interaction of the involved components.

Thanks to the ball drop test setup, in particular, it was shown that traditional windows can be extremely vulnerable to accidental impact events. This depends both on the type of glass that is used for non-structural building applications (i.e., monolithic glass, in place of laminated safety glass), as well as on the presence of mostly independent glass panels (due to unsealed, movable window components), that cannot take advantage of more efficient “load sharing effects” that are exploited by modern Insulated Glass Units. The final effect of these basic choices, as also shown in this paper, takes the form of a sudden and mostly total collapse mechanism for glass, in which large and glass shards and sharp splinters can be scattered through the room, and thus represent a severe risk for the occupants. The experimentally observed dynamic response for the selected traditional windows, on the other side, is strictly related to a multitude of geometrical and mechanical details, and especially the the linear connection of glass edges with the supporting frame members, but also the actual boundary condition, and possible additional effects due to high strain rates.

Both the static and dynamic experimental outcomes reported in this paper were thus further assessed with the support of geometrically simplified but mechanically accurate FE models. The sensitivity of basic modal parameters to the axial and rotational stiffness of the linear connection for glass edges was first explored, giving evidence of remarked mechanical effects on the overall response of the window. As far as geometrically simplified models are privileged for the analysis of composite glass systems, the lack detailed calibration for the interposed materials can result in unreliable static and dynamic predictions. At the same time, the attention of the numerical study proposed herein was focused on the analysis of maximum expected effects in traditional windows under hard body impact. Besides the limited number of test specimens, a relatively good correlation was generally observed for the developed FE models. The numerical analyses were found to capture the actual experimental peaks for the impact experiments, as a major effect of a detailed calibration of input details. The available dynamic experimental outcomes for the windows specimens at collapse, moreover, were used for the numerical analysis of local effects and derivation of the tensile resistance of annealed glass under the ball drop impact setup. This average value was found to agree with past literature results, with a mean dynamic increment in the range of ≈2, compared to static conditions. The same FE results, however, still confirmed the high variability of the same resistance value, hence representing a critical parameter for safe design purposes.

Compared to modern ordinary windows, finally, the examined traditional, timber-braced window solution typically resulted in a limited bending stiffness and resistance, thus in a pronounced vulnerability towards potential accidental events.

In this regard, it is thus expected that the current research study could be further extended to include a multitude of geometrical configurations and loading (especially impact) conditions of technical interest for design, and thus support the development of a set of efficient tools for the vulnerability assessment of existing, in-service glass windows for ordinary buildings.

Acknowledgments

This paper follows and extends, upon invitation, a previous ANCRiSST2019 workshop oral presentation from the same authors (14th International Workshop on Advanced Smart Materials and Smart Structures Technology, Rome, Italy). The Guest Editors of the Special Issue on Smart Structures and Systems are warmly acknowledged for the invited submission, as well as for the interest and positive evaluation of the research topic.

References

Aluplast (2020), http://bamareal.sk/aluplast/8-ideal-4000.html

Arexons® SEAL 5661, https://www.astorispa.it/downloads/download/16514/mastice-per-guarnizione-seal-5661-arexons-20032_1

Bedon, C. and Amadio, C. (2014), "Exploratory numerical analysis of two-way straight cable-net façades subjected to air blast loads", *Eng. Struct.*, **79**(11), 276-289. https://doi.org/10.1016/j.engstruct.2014.08.023

Bedon, C. and Amadio, C. (2020), "Mechanical analysis and characterization of IGUs with different spacers—part 1: experiments", *Glass Struct. Eng.* https://doi.org/10.1007/s40940-020-00122-w

Bedon, Ch. and Figuli, L. (2017), "An overview on current methods and trends for enhancing the blast resistance and protection of existing windows", *Transport Means - Proceedings of the International Conference 2017*, pp. 977-984.

Bedon, C., Kalamar, R. and Eliasova, M. (2017), "Low velocity impact performance investigation on square hollow glass columns via full-scale experiments and Finite Element analyses", *Compos. Struct.*, **182**, 311-325. https://doi.org/10.1016/j.compstruct.2017.09.055

Bedon, C., Zhang, X., Santos, F., Honfi, D., Kozłowski, M., Arrigoni, M., Figuli, D. and Lange, D. (2018), "Performance of structural glass facades under extreme loads – design methods, existing research, current issues and trends", *Constr. Build. Mater.*, **163**, 921-937. https://doi.org/10.1016/j.conbuildmat.2017.12.153

Bedon, C., Fasan, M. and Amadio, C. (2019), "Vibration analysis and dynamic characterization of structural glass elements with different restraints based on Operational Modal Analysis", *Buildings*, **9**(1), 13. https://doi.org/10.3390/buildings9010013

Bouzida, S., Nyoungue, A., Azari, Z., Bouaouadja, N. and Pluvinage, G. (2001), "Fracture criterion for glass under Impact loading", *Int. J. Impact Eng.*, **25**, 831-845. https://doi.org/10.1016/S0734-743X(01)00023-9

Brown, W. (1974), "A practicable formulation for the strength of glass and its special application to large plates", Tech. Rep. Publication No. NRC14372; National Research Council of Canada, Ottawa, Canada.

Chocron, S., Barnette, D.D., Holmquist, T.., Anderson Jr., C.E., Bigger, R.P. and Moore, T.Z. (2016) "Damage Threshold of Borosilicate Glass Under Plate Impact", *J. Dyn. Behavior Mater.*, **2**, 167-180. https://doi.org/10.1007/s40870-016-0056-4

EN 572–2 (2004), Glass in buildings – Basic soda lime silicate glass products, CEN, Brussels, Belgium.

Figuli, L. (2019), "Analysis, design and protection of blast loaded windows", Critical infrastructure protection: best practices and innovative methods of protection. NATO Science for Peace and Security Series - D: Information and Communication Security, 52, Amsterdam: IOS Press, 27-43. https://doi.org/10.3233/978-1-61499-964-5-27

Figuli, L., Zvaková, Z. and Bedon, C. (2017), "Design and analysis of blast loaded windows", *Procedia Eng.*, **192**, 177-182. https://doi.org/10.1016/j.proeng.2017.06.031

Figuli, L., Erdelyiová, R., Papán, D. and Papánová, Z. (2020), "Resistance of glass window subjected to high velocity soft impact", *MATEC Web of Conferences*, 313, 00027, DYN-WIND'2020. https://doi.org/10.1051/matecconf/202031300027

Kruszka, L. and Rekucki, R. (2020), "Experimental analysis of impact and blast resistance for various built security components", Soft target protection, NATO Science for Peace and Security Series C: Environmental Security, Springer, p. 211-239.

Meyers, G.E. (1994), BLASTOP version 1.4, US Department of Energy.

Mohagheghian, I., Wang, Y., Zhou, J., Yu, L., Guo, X., Yan, Y., Charalambides, M.N. and Dear, J.P. (2017), "Deformation and damage mechanisms of laminated glass windows subjected to high velocity soft impact", *Int. J. Solids Struct.*, **109**, 46-62. https://doi.org/10.1016/j.ijsolstr.2017.01.006

Papán, D. and Papánová, Z. (2020), "Analysis of static and dynamic parameters of the wooden window glass frame", *MATEC Web of Conferences*, **313**. https://doi.org/10.1051/matecconf/202031300028

Pyttel, T., Liebertz, H. and Cai, J. (2011), "Failure criterion for laminated glass under impact loading and its application in finite element simulation", *Int. J. Impact Eng.*, **38**, 252-263. https://doi.org/10.1016/j.ijimpeng.2010.10.035

Simulia (2020), ABAQUS computer software, v. 6.14, Dassault Systemes, Providence, RI, USA.

SSG - Special Services Group (1997), Explosion Protection. Glazing Hazard Guide – Charts, Security Facilities Executive, Report SSG/EP/3/97.

Wang, X., Yang, J. and Xu, H. (2018), "Experimental investigation on the Impact Resistance of Laminated Glass with Various Glass Make-ups", *Challenging Glass 6 – Conference on Architectural and structural Applications of Glass*, **6**, 475-484. https://doi.org/10.7480/cgc.6.2205

Xue, L., Coble, C.R., Lee, H., Yu, D., Chaparala, S. and Park, S. (2013), "Dynamic analysis of the thin glass under ball drop impact with new metrics", *Proceedings of the ASME 2013 International Technical Conference and Exhibition on Packing and Integration of Electronic and Photonic Microsystems InterPACK2013*. https://doi.org/10.1115/IPACK2013-73291